A DENSITY DEPENDENT MODEL OF INFLUENZA INFECTION RATE

by

Hope Sage

Submitted in partial fulfillment of the
requirements for Departmental Honors in
the Department of Physics & Astronomy
Texas Christian University
Fort Worth, Texas

May 6, 2024

A DENSITY DEPENDENT MODEL OF INFLUENZA INFECTION RATE

Project Approved:

Supervising Professor: Hana Dobrovolny, Ph.D.

Department of Physics & Astronomy

Magnus Rittby, Ph.D.

Department of Physics & Astronomy

Sergei V. Dzyuba, Ph.D.

Department of Chemistry & Biochemistry

Abstract

The most common viral dynamics models for analyzing viral infections assume even spatial distribution between virus particles and uninfected target cells. However, throughout an infection, the spatial distribution of virus and cells changes. Initially, virus and infected cells are localized so that a target cell in an area with lower virus presence will be less likely to be infected than a cell close to a location of viral production. A density-dependent infection rate has the potential to improve models that treat cellular infection probability as constant. Saturated Incidence, Beddington-DeAngelis, and Crowley Martin models were used to understand how density dependent parameters could impact the severity of an influenza infection. Parameter values were varied to understand implications of density constraints. For low density dependence, a steeper increase in virus and greater viral peak was predicted. Initial localization of infected cells likely slows the progression of infection. The model demonstrates that accounting for density dependence when analyzing influenza infection severity can result in an altered expectation for viral progression. A density-dependent infection rate provides a more complete view of the interaction between infected and uninfected cells.

1 Introduction

Influenza is a serious disease that affects many people worldwide every year with substantial illness and financial burden. Each flu season, approximately 8 percent of the United States population suffers from the flu (1). The total yearly economic impact of influenza on the US economy is upwards of 10 billion dollars (2). Globally, influenza is estimated to account for 650,000 deaths annually (2). Given the severity of medical and economic impacts from influenza, increasing understanding of viral progression is essential in order to reduce the extent of symptoms associated with infection and to improve clinical outcomes.

Mathematical modeling provides a cost-effective method for analyzing, predicting, and understanding viral kinetics. Models are frequently developed to account for a wide range of viruses, antiviral drugs, immune response modifications (3) , and age differentiated outcomes (4). By employing mathematical models, clinicians and researchers can be better equipped to understand how untreated disease will progress as well as provide a foundation for testing treatment options theoretically before exploring more resource intensive actions including animal and human laboratory testing. Biophysical models contribute to increased understanding of progressions of disease and can result in better estimations of predicted infection severity (5). Enabled by a better understanding of viral kinetics, drug efficacy and the effect of treatments can be estimated (5).

Work done by Baccam et al. (6) laid a foundation for applying mathematical models to H1N1 influenza progression. A system of four differential equations that accounts for changes in populations of uninfected target cells, cells in a noncontagious phase of intracellular viral replication, infected cells, and virus was used. Through data fitting, accounting for an eclipse phase was found to provide an effective method for accounting for the delay between an uninfected cell's contact with virus and time of the cell becoming infected. However, the model assumes equal spatial contact between all cell types, which is inconsistent with biophysical understanding of viral progression. Early on in an infection, virus is highly localized and does not have equal surface area contact with all uninfected cells.

Attempts have been made at quantifying and analyzing the impact of biophysical understanding of viral kinetics on projected disease progression. One approach involved modifying clearance rates of infected cells to account for changes in spatial distribution between uninfected cells, infected cells, eclipsed cells, and virus (7). In addition to a well-mixed assumption, most viruses do not have a complete set of genome sequences resulting in a combination

of semi-infectious and fully infected particles. Work done on evaluating the impact of Semi-Infectious Particles (SIPS) and heterogeneity throughout the course of infection (8) found that modifications in spatial arrangement were essential to accurately represent experimental data. Density-dependent contact rates have been frequently explored in epidemiology (9) as a means of understanding how disease spreads between infected and uninfected populations as a result of human to human contact rates. Mathematical models exploring density-dependent constraints have also been explored in an attempt to better understand HIV disease dynamics using a Beddington-DeAngelis function (10).The Beddington De-Angelis model and Crowley-Martin Incidence model have been used in modeling viruses across a variety of contexts (11),(12). Here, we investigate three models of density-dependent infection to assess their impact on the time course of influenza infection. In order to quantify the impact of changes in spatial distribution on aspects of virus progression, parameters constraining uninfected target cell growth based on changes in uninfected target cells and virus may provide increased accuracy to a system of differential equations modeling viral progression. By varying density dependent constraints, the impact of spatial heterogeneity on infection severity and duration can be analyzed. Measurements of the viral titer curve and fixed points of the system are measured in the context of a range of density dependent values in an attempt to align biophysical understanding with mathematical modifications.

2 Methods

2.1 Density Dependent Incident Functions

The most common viral dynamics models for analyzing viral infections assume even spatial distribution between virus particles and target cells. However, throughout an infection spatial distribution of virus and cells changes. A standard viral kinetics model was developed using four differential equations describing change in uninfected target cells as proportional to interaction between uninfected target cells and virus particles by Baccam et al. (6). Uninfected target cells that come in contact with virus particles enter an eclipse phase where virus is replicating within the cell and then becomes infectious at a rate $\frac{1}{k}$. Once infectious, cells produce virus at rate, p. All infectious cells are assumed to die after a time of $\frac{1}{\delta}$, while virus is cleared at a rate of c, as demonstrated in the standard viral kinetics model (6). Model parameter values are shown in Table 1.,

$$\begin{aligned}
\frac{dT}{dt} &= -\beta VT \\
\frac{dE}{dt} &= \beta VT - kE \\
\frac{dI}{dt} &= kE - \delta I \\
\frac{dV}{dt} &= pI - cV.
\end{aligned}$$

In order to account for density dependence, parameters were analyzed through three density dependent mathematical functions for constrained viral progression. Models considered were a Saturated Incidence function, Beddington De-Angelis function, and Crowley-Martin Incidence model. Both the Beddington De-Angelis model and Crowley-Martin Incidence model are based on systems of differential equations commonly used to assess predator-prey interactions (13). The Crowley-Martin model has also been frequently used to fit epidemiological conditions (14).

- Saturated Incidence Model:

$$\begin{aligned}
\frac{dT}{dt} &= \frac{-\beta VT}{1+\alpha V} \\
\frac{dE}{dt} &= \frac{-\beta VT}{1+\alpha V} - kE \\
\frac{dI}{dt} &= kE - \delta I \\
\frac{dV}{dt} &= pI - cV
\end{aligned}$$

- Beddington De-Angelis Model:

$$\begin{aligned}
\frac{dT}{dt} &= \frac{-\beta VT}{1+\gamma T+\alpha V} \\
\frac{dE}{dt} &= \frac{-\beta VT}{1+\gamma T+\alpha V} - kE \\
\frac{dI}{dt} &= kE - \delta I \\
\frac{dV}{dt} &= pI - cV
\end{aligned}$$

Table 1: Model parameters, taken from Baccam et al. (6).

Variable	Value	Unit
β	Infection Rate	3.2×10^{-5} $(\text{TCID}_{50}/\text{mL} \cdot \text{d})^{-1}$
p	Viral Production Rate	4.6×10^{-2} $\text{TCID}_{50}/\text{mL} \cdot \text{d}$
k	(Transition Time to Infectious Cell)$^{-1}$	4.0 /d
δ	(Infected Cell Life Span) $^{-1}$	5.2 /d
c	Viral Clearance Rate	5.2 /d
V_0	Initial Viral Titer	7.5×10^{-2} $\text{TCID}_{50}/\text{mL}$
T_0	Target Cells	$4\times$ 10^8 cells

- Crowley-Martin Incidence Model:

$$\begin{aligned}
\frac{dT}{dt} &= \frac{-\beta VT}{(1+\gamma T)(1+\alpha V)} \\
\frac{dE}{dt} &= \frac{-\beta VT}{(1+\gamma T)(1+\alpha V)} - kE \\
\frac{dI}{dt} &= kE - \delta I \\
\frac{dV}{dt} &= pI - cV
\end{aligned}$$

2.2 Model Parameters

Parameter values for the H1N1 flu virus (6) were used (Table 1), and α and γ were varied across a range to see how parameter variations affected measures of viral severity. In the Saturated Incidence model, α was varied from 10^{-3} to 10^3 with 100 steps on a log scale. In the Beddington De-Angelis and Crowley-Martin Incidence models, α was simulated from 10^{-3} to 10^3 with 100 steps on a log scale and γ was simulated from 10^{-15} to 10^{-7} in 100 steps on a log scale to mimic possible physiological ranges. Other model parameters were taken from fits of the standard model to patient data from Baccam et al. (6) and are given in Table 1. Systems of differential equations for each model were solved using `scipy.odeint`, and stored in array form to be used for calculating measures of the curve.

2.3 Calculations for Measures of the Curve

Several measures of the viral titer curve were calculated to characterize how the infection changes with changes in density dependence (Fig. 1). Viral peak was determined by locating the maximum value of the curve given an initial amount of virus as 7.5×10^{-2} $\text{TCID}_{50}/\text{mL}$

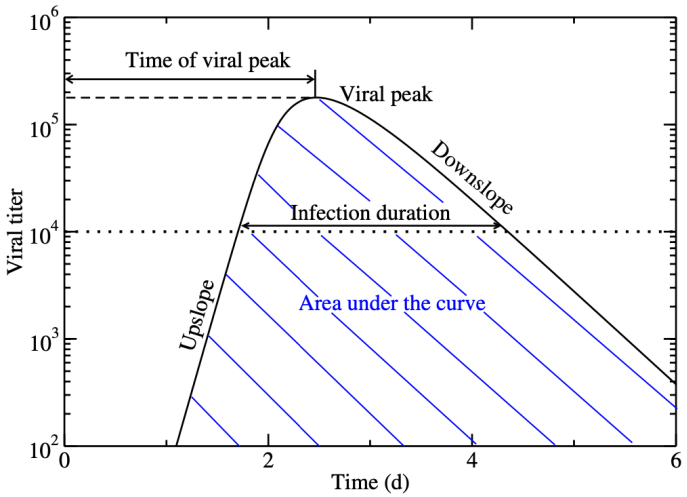

Figure 1: Measured aspects of the viral titer curve as related to changes in density dependence

and 4 $\times 10^8$ initial uninfected target cells within the ranges for both α and γ. The time at which this maximum occurred was found by locating the correlated time value to the maximum value, which serves as a measure of time to peak and provides insight into how fast the infection is progressing.

The slope of the viral titer curve was found by plotting virus concentration vs. time and using a linear least squares fit over the the primary time points of ascent or descent of the viral titer curve. For each function, selected ranges varied slightly. Ranges were selected by identifying initial substantial increase in virus as a starting point and stopped where the slope of ascent began to approach zero. Downslope ranges were started where the viral titer curve was past maximum and began to experience descent as compared to immediately post peak and ended where slope was approaching zero. These ranges were selected to allow for a linear fit of the viral titer curve. The duration of infection for each model was found by subtracting the final time point from which virus was above a threshold of 10 TCID_{50}/ml from the time that the viral titer initially rose to the threshold value. The area under the curve (AUC) was found using 300 trapezoidal approximations and verified with Simpson's rule,

$$\text{AUC} = \frac{b-a}{2n}(V_0 + V_f + 2\sum(V_{1:n-1})),$$

where n is the number of steps used to simulate time - 1, b and a are the final and initial

time values, and V represents virus.

The basic reproduction number, R_0, describes how many target cells an infected cell will infect. R_0 was calculated using the Next Generation Matrix method where each system was split into infected and non infected states (15). Equations $\frac{dE}{dt}$, $\frac{dI}{dt}$, and $\frac{dV}{dt}$ for each model were split into F and V matrices, where F and V were partial derivative matrices. F represents the rate at which cells become infected and V represents transfer between or out of the infected state. F matrices were then multiplied by the inverse of V. The dominant eigenvalues of each matrix were then calculated to find the R_0.

3 Results

Systems of differential equations that assume well-mixed spatial distributions were modified by varying parameters that constrain viral growth to understand how changes in spatial contact affect viral progression. Three different density dependent ordinary differential equation systems were used. Key aspects of the viral titer curve were measured to understand possible outcomes of viral kinetics when density dependence is accounted for in models. Peak viral load, timing of peak viral load, viral upslope, viral downslope, area under the curve, and infection duration were measured on the viral titer curve across varied ranges of α and γ. In addition, practical applications were explored by assessing the minimum effectiveness necessary for a drug to successfully eliminate infection for each model across ranges of density dependence. Drug efficacy was determined from analyzing the steady states of the system which were calculated using a next generation matrix method. Increasing values of density dependence generally slowed progression and severity of virus.

3.1 Saturated Incidence Model

Changes in viral titer characteristics for the Saturated Incidence model are shown in Fig. 2. As α increases, the viral maximum decreases, but time to maximum increases before reaching a point where density dependence is so high that the infection does not occur. Viral upslope generally decreases with greater density dependence. At higher density dependence, the downslope becomes rapidly less steep before leveling off towards zero. Infection duration occurs in a two-phase manner that rapidly drops to zero for higher density dependent values. Area under the curve was lower for greater density dependence. Results suggest

that predicted measures of infection severity for higher density dependence in the saturated Incidence model result in a less severe infection with lower maximum viral load and slower viral growth compared to the model in (6).

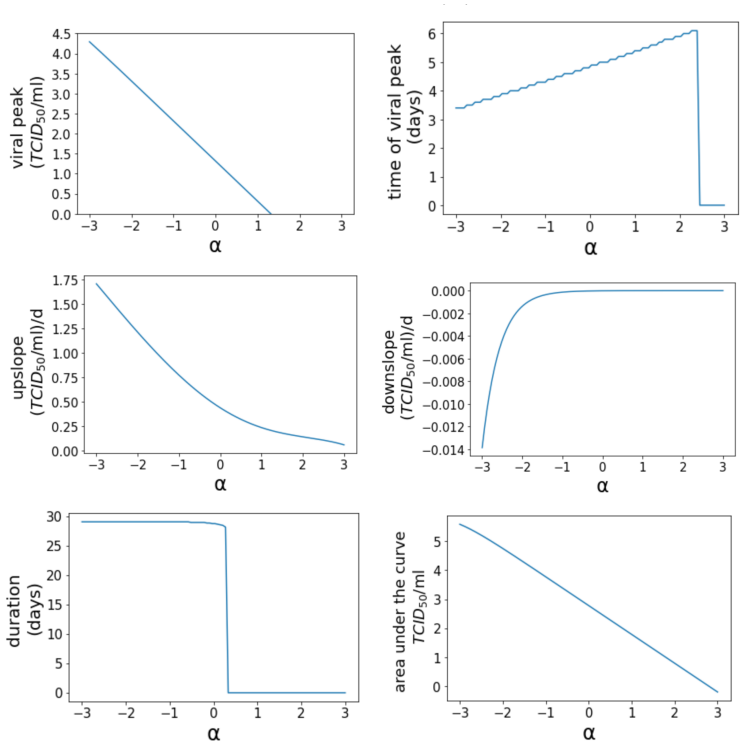

Figure 2: Measurements of the (top left) maximum viral load (log scaled), (top center) time of maximum, (top right) viral upslope, (bottom left) viral downslope, (bottom center) infection duration, and (bottom right) area under the curve (log scaled) of the Saturated Incidence Model when varying the parameter α from 10^{-3} to 10^{3} on a log scale.

3.2 Beddington De-Angelis Model

Figure 3 shows predicted trends in viral titer curve measurements based on variations in α and γ. For the Beddington De-Angelis Model, viral peak predicted values are higher for lower density dependence. Time of peak shows minimal variation related to density dependence until a maximum α or γ value occurs that results in no infection. As a maximum γ value that allows for infection to occur is approached, a time delay in viral peak is observed. As α gets larger, no time delay is observed. This indicates higher density dependence is associated with reduced ability of the infection to spread. The predicted viral upslope is steeper for lower density dependence and viral downslope rapidly descends towards zero excluding high density dependence values of γ. Duration of infection distinctly levels off to zero for higher

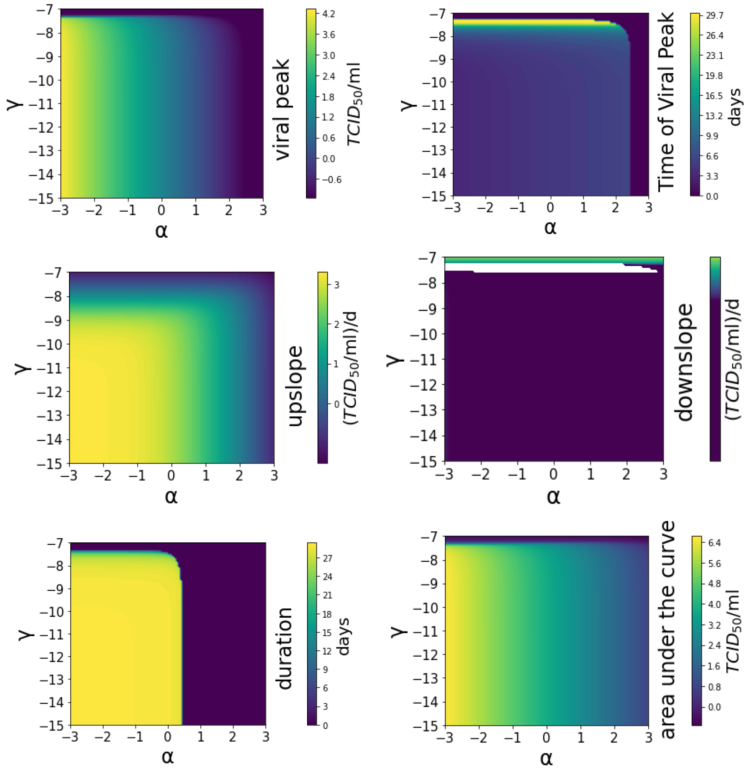

Figure 3: Heatmaps of the (top left) maximum viral load (log scaled), (top center) time at maximum, (top right) viral upslope, (bottom left) viral downslope, (bottom center) infection duration, and (bottom right) area under the curve (log scaled) of the Beddington DeAngelis model based on varying density dependent parameters (α and γ) on a log scale.

α values in an abrupt manner rather than a gradual decline. Area under the curve appears to be lower for greater density dependence values of α with no infection occurring beyond a maximum value of γ. The Beddington-DeAngelis model demonstrates that increases in density dependence slow viral progression and decrease the maximum total amount of virus by limiting the ability of infection to spread.

3.3 Crowley-Martin Incidence Function Results

The Crowley-Martin Incidence function demonstrates similar predicted trends to the Beddington De-Angelis Model, as shown in Fig. 4. For lower density dependence, viral maximum is greater. Timing of the peak remains consistent despite varied density dependence values until reaching a maximum value of α or γ where the infection no longer occurs. As this value is approached for γ, a delayed time to viral peak is briefly seen for higher γ values but this tendency is not observed as α values approach the boundary. For lower density dependence, viral upslope to maximum is greater indicating a faster progression of infection. Downslope

rapidly approaches zero regardless of density variation. Very high levels of density dependence for γ indicate a minor extension in downslope but the same is not observed for α. At high α values, predicted values for infection duration experience an abrupt drop to zero. For high γ values, there is a brief shortening in infection duration as values approach a maximum value beyond which no infection occurs. This indicates that infection duration remains fairly constant despite density variation until a point is reached where the virus cannot spread to produce an infection. Area under the curve was lower for greater density dependence values for α. For γ variation, changes in simulated area under the curve were not observed until γ values reach a maximum value inhibiting infection occurrence. These trends predict a less severe overall infection for greater density dependence.

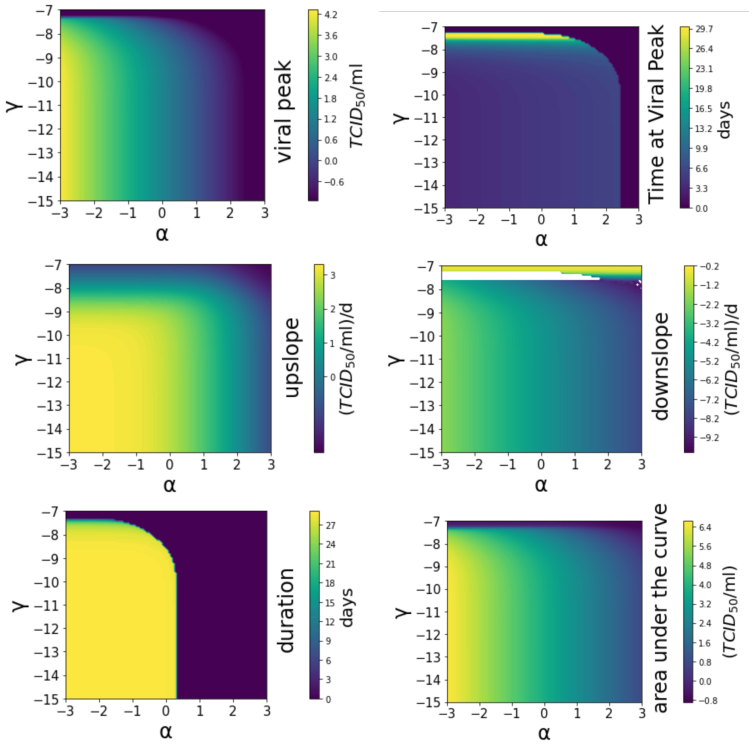

Figure 4: Heatmaps of the (top left) maximum viral load (log scaled), (top center) time at maximum, (top right) viral upslope, (bottom left) viral downslope, (bottom center) infection duration, and (bottom right) area under the curve (log scaled) of the Crowley Martin Incidence Model based on varying density dependent parameters (α and γ) on a log scale.

3.4 Basic Reproduction Number

The basic reproduction number, R_0, of the infection was calculated using the next generation matrix method and indicates the number of cells a single infectious cell will infect (16). For

R_0 values greater than one, viral load will continue to increase and the infection will become more severe. For R_0 values below one, the viral load will continue to decrease and the infection will regress. As as result, R_0 is crucial for understanding how the infection will continue to develop and for developing effective treatment options. The next generation matrix method splits each differential equation system into F and V matrices representing new infections and transitions between or away from infected states. F and V matrices used in R_0 calculations are given below. The R_0 is the largest eigenvalue of the next generation matrix.

- Saturated Incidence model:

$$F = \begin{bmatrix} 0 & 0 & \frac{\beta T_0(1+\alpha V_0)-\alpha(\beta T_0 V_0)}{(1+\alpha V_0)^2} \\ 0 & 0 & 0 \\ 0 & 0 & 0 \end{bmatrix} \quad V = \begin{bmatrix} k & 0 & 0 \\ -k & \delta & 0 \\ 0 & -p & c \end{bmatrix}$$

$$FV^{-1} = \frac{\beta T_0(1+\alpha V_0)-\alpha(\beta T_0 V_0)}{(1+\alpha V_0)^2} \begin{bmatrix} \frac{p}{\delta c} & \frac{p}{\delta c} & \frac{1}{c} \\ 0 & 0 & 0 \\ 0 & 0 & 0 \end{bmatrix}$$

  Using cofactor expansion along the the first column, the resulting characteristic equation is

$$F(\lambda) = \left(\frac{\beta p T_0(1+\alpha V_0) - \alpha\beta p T_0 V_0}{(1+\alpha V_0)^2 \delta c} - \lambda \right) (0-\lambda)(0-\lambda)$$

  .

- Beddington De-Angelis model:

$$F = \begin{bmatrix} 0 & 0 & \frac{\beta T_0(1+\gamma T_0+\alpha V_0)-\alpha(\beta T_0 V_0)}{(1+\gamma T_0+\alpha V_0)^2} \\ 0 & 0 & 0 \\ 0 & 0 & 0 \end{bmatrix} \quad V = \begin{bmatrix} k & 0 & 0 \\ -k & \delta & 0 \\ 0 & -p & c \end{bmatrix}$$

$$FV^{-1} = \frac{\beta T_0(1+\gamma T_0+\alpha V_0)-\alpha(\beta T_0 V_0)}{(1+\gamma T_0+\alpha V_0)^2} \begin{bmatrix} \frac{p}{\delta c} & \frac{p}{\delta c} & \frac{1}{c} \\ 0 & 0 & 0 \\ 0 & 0 & 0 \end{bmatrix}$$

  Using cofactor expansion along the the first column, the resulting characteristic

equation is

$$F(\lambda) = \left(\frac{\beta p T_0 (1 + \gamma T_0 + \alpha V_0) - \alpha \beta p T_0 V_0}{(1 + \gamma T_0 + \alpha V_0)^2 \delta c} - \lambda \right) (0 - \lambda)(0 - \lambda)$$

.

- Crowley Martin model:

$$F = \begin{bmatrix} 0 & 0 & \frac{\beta T_0 (1+\alpha V_0)(1+\gamma T_0) - B T_0 V_0 (\alpha + \alpha\gamma T_0)}{(1+\gamma T_0)(1+\alpha V_0)^2} \\ 0 & 0 & 0 \\ 0 & 0 & 0 \end{bmatrix} \quad V = \begin{bmatrix} k & 0 & 0 \\ -k & \delta & 0 \\ 0 & -p & c \end{bmatrix}$$

$$FV^{-1} = \frac{\beta T_0 (1 + \alpha V_0)(1 + \gamma T_0) - \beta T_0 V_0 (\alpha + \alpha \gamma T_0)}{(1 + \gamma T_0)(1 + \alpha V_0)^2} \begin{bmatrix} \frac{p}{\delta c} & \frac{p}{\delta c} & \frac{1}{c} \\ 0 & 0 & 0 \\ 0 & 0 & 0 \end{bmatrix}$$

Using cofactor expansion along the the first column, the resulting characteristic equation is

$$F(\lambda) = \left(\frac{\beta p T_0 (1 + \alpha V_0)(1 + \gamma T_0) - \alpha \beta p T_0 V_0 (1 + \gamma T_0)}{(1 + \gamma T_0)(1 + \alpha V_0)^2 \delta c} - \lambda \right) (0 - \lambda)(0 - \lambda)$$

.

R_0 values are substantially lower for simulations of greater density dependence than higher density dependence (Fig. 5). Lower R_0 values indicate a less extensive spread of virus within the body which supports minimized contact between target cells and virus particles. As a result, spatially localized mixtures predict a less rapid progression of influenza than well-mixed particle distribution.

3.5 Infecting Time

Measures of infecting time were also calculated in order to determine the time required for a virus that has been produced to leave a cell and infect another cell. This provides similar insight to the R_0 of the system by increasing understanding of the effect of speed of viral spread. Steps for calculations were followed from González-Parra et al (17).

Virus is produced at rate ρ and cells going from uninfected states to an eclipsed state as a result of newly produced virus is described by $\frac{dE}{dt}$. To find the infecting time (t_{inf}), time

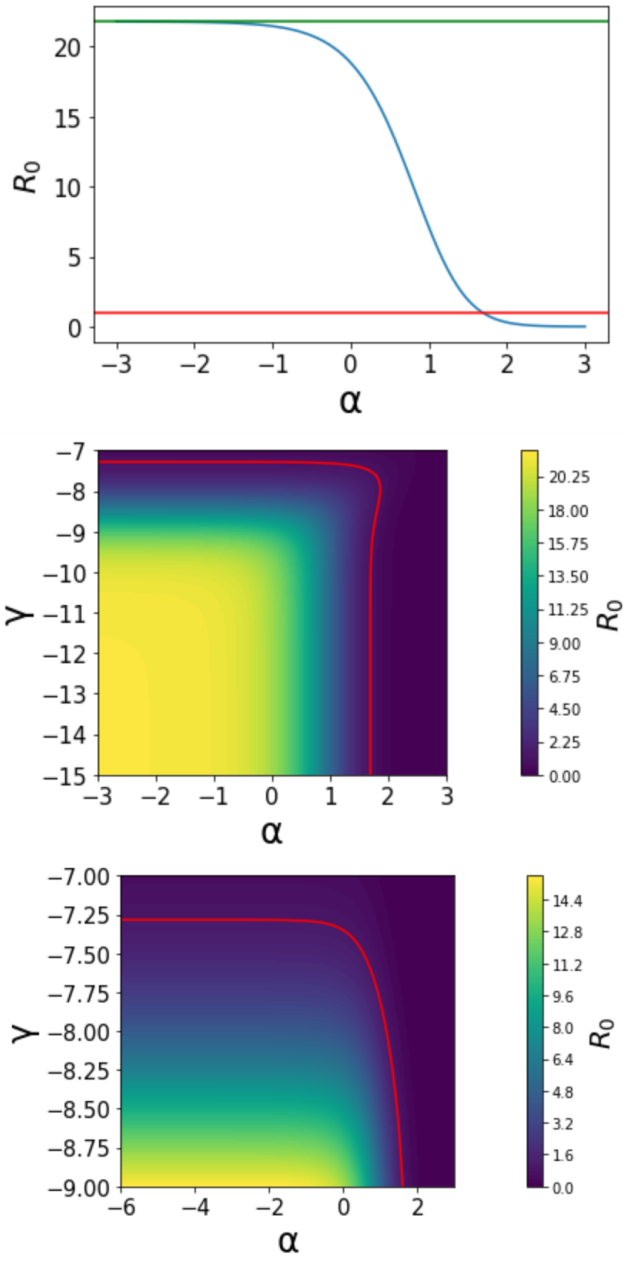

Figure 5: R_0 for different density-dependent models. (top) R_0 for saturated Incidence, (middle) R_0 for BDA model, and (bottom) R_0 for CM model. $R_0 = 1$ is labeled in red and R_0 calculated from the model not accounting for density dependence is in green (6).

between virus production and infection of an uninfected cell is being analyzed so the rate at which cells leave the eclipsed phase for the infected phase is not considered. We assume that viral clearance during this time is negligible, therefore,

$$\frac{dV}{dt} = p$$

and

$$\frac{dE}{dt} = \frac{\beta V T_0}{1 + \alpha V}.$$

for the saturated Incidence model. Integrating both equations,

$$\begin{aligned} V(t) &= pt \\ \int_0^1 dE &= \int_0^{t_{\text{inf}}} \frac{\beta T_0 pt}{1 + \alpha pt} dt \\ 1 &= \beta T_0 p \int_0^{t_{\text{inf}}} \left(\frac{1}{\alpha p} - \frac{1}{\alpha p(\alpha pt + 1)} \right) dt \\ 1 &= \beta T_0 \left(\frac{t_{\text{inf}}}{\alpha p} - \frac{1}{\alpha^2 p} \int_0^{t_{\text{inf}}} \frac{1}{\alpha pt + 1} dt \right) \\ 1 &= \frac{\beta T_0 (\alpha p t_{\text{inf}} - \ln |\alpha p t_{\text{inf}} + 1|)}{\alpha^2 p}. \end{aligned} \tag{1}$$

Following the same logic as above, the infecting time relationship for the Beddington De-Angelis Model can be integrated from:

$$\frac{dV}{dt} = p$$

and

$$\frac{dE}{dt} = \frac{\beta T_0 V}{1 + \alpha V + \gamma T_0}.$$

Integrating gives

$$\begin{aligned} \int_0^1 dE &= \int_0^{t_{\text{inf}}} \frac{\beta T_0 pt}{1 + \alpha pt + \gamma T_0} dt \\ 1 &= \beta T_0 p \int_0^{t_{\text{inf}}} \left(\frac{1}{\alpha p} + \frac{-\gamma T_0 - 1}{\alpha p(\alpha pt + \gamma T_0 + 1)} \right) dt \end{aligned}$$

Following long division and integration, the infecting time relationship becomes:

$$1 = \frac{\beta T_0}{\alpha^2 p}\left(\alpha p t_{\text{inf}} + (\gamma T_0 + 1)\ln\left|\frac{1+\gamma T_0}{\alpha p t_{\text{inf}} + \gamma T_0 + 1}\right|\right). \quad (2)$$

For the Crowley Martin model,

$$\begin{aligned} V &= pt \\ \int_0^1 dE &= \int_0^{t_{\text{inf}}} \frac{\beta T_0 pt}{(1+\alpha pt)(\gamma T_0 + 1)} dt \\ 1 &= \frac{\beta T_0 p}{\gamma T_0 + 1}\int_0^{t_{\text{inf}}}\left(\frac{1}{\alpha p} - \frac{1}{\alpha p(\alpha pt + 1)}\right) dt \\ 1 &= \frac{\beta T_0}{\gamma T_0 + 1}\left(\frac{t_{\text{inf}}}{\alpha} - \frac{1}{\alpha^2 p}\int_0^{t_{\text{inf}}} \frac{1}{\alpha pt + 1} dt\right) \\ 1 &= \frac{\beta T_0}{\alpha^2 p(1+\gamma T_0)}\left(\alpha p t_{\text{inf}} - \ln\left|\frac{1+\gamma T_0}{(\alpha p t_{\text{inf}} + 1)(1+\gamma T_0)}\right|\right). \end{aligned} \quad (3)$$

For all three models, greater density dependence was associated with longer infecting times (Fig. 6), indicating that increased heterogeneity impedes the virus' predicted ability to infect other cells.

3.6 Drug Efficacy Measures

Based on the R_0, the minimal drug efficacy needed to cure an infection can be found. We define the efficacy of a drug, ϵ, as the fractional reduction in a particular viral replication process. When modeling the effect of a drug, we multiply the affected parameter by $(1-\varepsilon)$ where ϵ is a number between 0 and 1. This results in the R_0 value also being reduced by $(1-\epsilon)$. Recall that when R_0 is below 1, the infection's growth experiences decline ((18)). As a result, the minimal efficacy of a drug is the effectiveness required to reduce the infection's R_0 below one and can be found by the following relationship,

$$\epsilon = 1 - \frac{1}{R_0}.$$

The minimal drug efficacies needed to cure are shown as functions of density dependence in Figure 7. For the Saturated Incidence Model as values of α increase, the minimal effective dose of a drug to send the infection into remission declines, but only at high values of α. This indicates that a lower dose of a drug may be effective when density dependence is considered. For the Beddington De-Angelis model, minimal effective dose remains constant

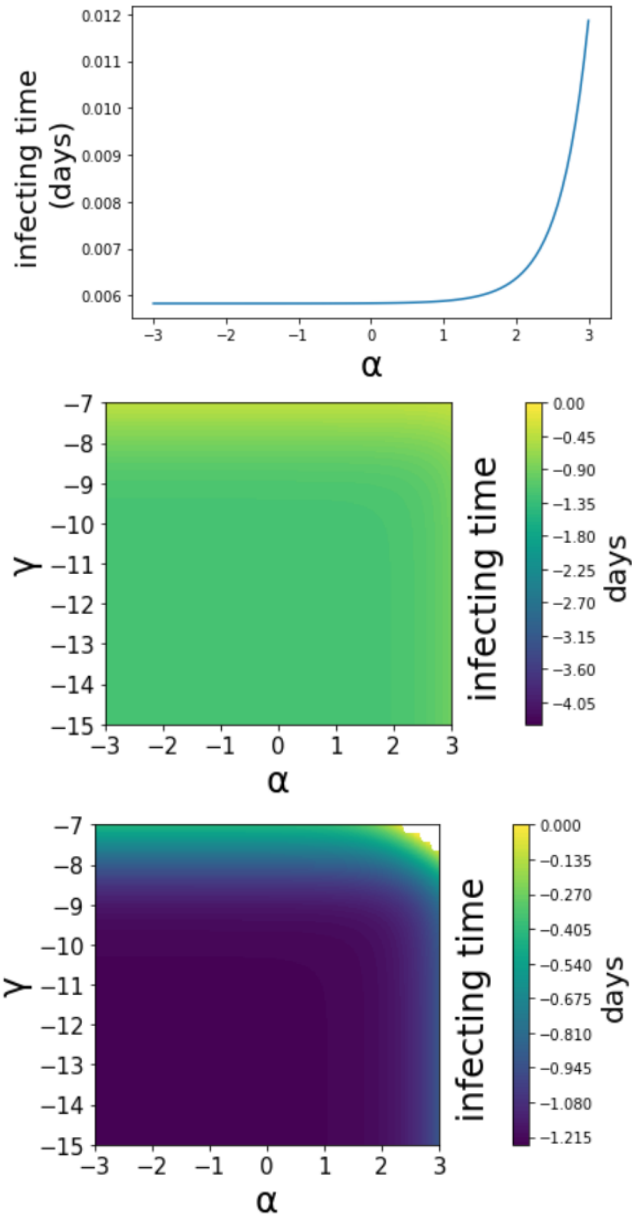

Figure 6: Infecting times for for varied density dependence. Saturated Incidence (top), Beddington De-Angelis (middle), and Crowley-Martin (bottom), where both the Beddington De-Angelis and Crowley-Martin models are graphed on a log scale.

and high regardless of density dependence until a threshold value of α and γ are reached in which case minimal effectiveness substantially decreases. This indicates that density dependence does not noticeably affect minimal efficacy until a threshold parameter value is reached where necessary effectiveness decreases rapidly. For the Crowley-Martin model, a similar effect of reaching a threshold value that results in subsequent decline in minimal effective dose required to eliminate infection is observed for high density dependent values of γ but not for α.

4 Discussion

Because the Saturated Incidence model only analyzes changes in α, trends in infection progression within the model can directly be tied to changes within the range of one density dependence value. The Beddington De-Angelis model and Crowley-Martin Incidence model both rely on changes in multiple measures of density dependence. The Beddington De-Angelis model primarily experiences density dependence associated changes with changes in α. In the Crowley-Martin Incidence model, γ has a slightly greater constraining effect on virus than it does in the Beddington De-Angelis model. Changes in density dependence are impacted by changes in both variables.

Results for incorporation of density dependence alter the predicted progression of virus when compared to the basic model (6). Predicted measures of the influenza viral titer curve vary based on variations in parameterized constraints that represent density dependence. A general trend for viral progression as observed by all three considered Incidence functions suggests a decrease in maximum infection severity as a result of density considerations. Measured aspects of the viral titer curve demonstrate a slowed viral progression. The slowed initial progression of virus with higher density dependence supports spatial heterogeneity in the initial stages of infection.

For greater density dependence, viral peak values decrease which indicates a less severe infection at the peak of the infection. Time at which the viral peak occurs indicates a maximum density dependence beyond which no infection occurs. This is also reflected in the slope leading from initial infection to viral maximum. Since virus progresses by contact between uninfected target cells and virus particles, when virus particles have access to more uninfected target cells, the rate of infection progression is materially greater.

Mathematical modeling provides enhanced ability to gain insight into biophysical phe-

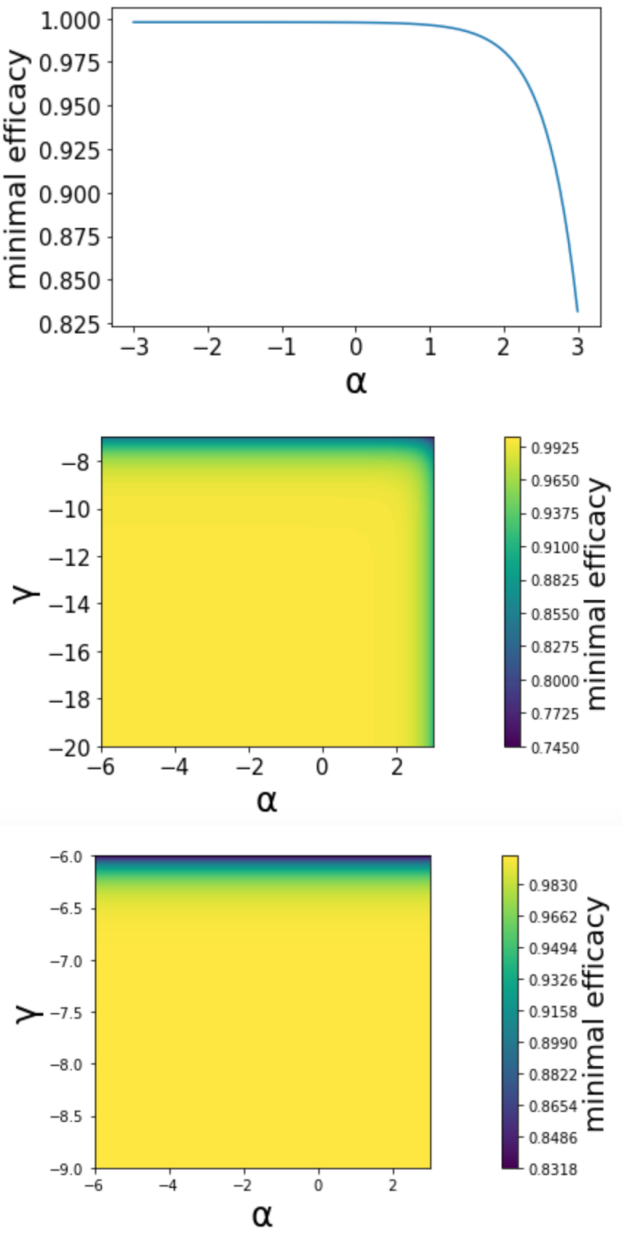

Figure 7: Minimal Drug efficacy required to send infection into decline for different models as a function of varied density dependent parameters. Minimal efficacy for varied density dependence Saturated Incidence (top), Beddington De-Angelis (middle), and Crowley-Martin (bottom).

nomena. Systems of ordinary differential equations are used to model the dynamics of viral progression in epidemiology (9) and within host to provide insight into disease progression while requiring relatively low input of financial resources. Proposed models of how biological understanding of infections maps to mathematical quantification allow for enhanced thought surrounding treatment development and preventative measures. Understanding key aspects of viral progression including the rate of increase of infection, timing of key infection measures, viral stability, and equilibrium points at which virus will continue to grow or diminish allows for optimal medical practice for influenza treatment.

The purpose of this paper is to modify an existing, frequently used, set of differential equations (6) that analyze H1N1 progression. The original model assumes virus and cells are well-mixed and spatially heterogeneous; we explored density-dependent infection rates that are consistent with biological understanding of the spatial distribution between uninfected cells and virus throughout the course of infection. Experimental evidence supports spatial heterogeneity throughout influenza progression (19). Attempts have been made at modifying commonly used ordinary differential equation based viral kinetics models to improve accurate mathematical representation of disease (20), (7), (21). Results in this paper for simulated viruses using ODE systems that represent a spatially heterogeneous distribution across a variance of physiological ranges indicate lower infection severity with increasing density dependence. Increasing density dependence reduces probability of contact between uninfected cells and virus especially early in an infection. Due to the localization of virus, surface area contact is lower than the well-mixed assumption for an equal quantity of virus. This results in a lower simulated value for expected viral peak because the rate of infection of target cells is reduced while the rate of clearance and death of infected cells is not experiencing the same reduction as a result of density dependence. Indications of changing viral dynamic predictions as a result of altered density dependence highlight the need for further exploration of factors affecting current quantitative understanding of influenza disease progression.

While mathematical models are commonly relied upon by experts in epidemiology to understand, predict, and modify aspects of the spread of disease, measurement error is a key challenge when modeling viral progression within the body (3). Numerical measures and initial conditions for influenza experience nontrivial error margins and variability among individuals. Data fitting to specific variations is challenging to collect for internal virus dy-

namics and constants used are often relative (3). As a result of challenges in measurement, modifying mathematical models to be consistent with improved quantitative biological understanding of virus progression has the potential to minimize error in model analysis and increase accuracy in understanding of future outcomes (5), (4).

Extending mathematical models to provide more insight into specific clinical context may allow for more strategic treatment development for patients. Minimal necessary effective doses of drugs for viral clearance as predicted by simulated viruses may serve as a valuable benchmark into drug development. Better understanding of viral dynamics may also provide enhanced insight into treatment options. While this work indicates a more rapid increase in virus, increasing viral max, greater area under the curve, and a larger R_0 value for lower density dependence, there are many other factors that contribute to infection severity and change the viral titer curve. Patient physiological conditions, initial virus concentration, immune response differences, comorbidities, and environmental factors all alter disease progression (21). As a result, a one-model fits all approach to influenza disease progression in treatment decisions lacks specificity to the individual.

Simulated viruses offer a window into how biophysical understanding aligns with predicted alteration in virus progression. Further work should include combining density dependent models with other constraints to improve accuracy for specified biological understanding including viral clearance rates, effectiveness of infection variation between infected particles, potential comorbidities, and medical treatment intervention. Implementing mathematical models that quantitatively include analysis of the immune response, which is often ignored due to the relatively short time duration of influenza progression, may improve biophysical understanding over target-cell limited models (3). Further, accuracy could be improved by fitting clinical data from human studies with measured viral titer curves to the model as a means of understanding which density dependent models most accurately represent influenza dynamics (5), (4).

References

[1] Centers for disease control and prevention, seasonal flu microsite, Aug 2022.

[2] Caroline de Courville, Sarah M. Cadarette, Erika Wissinger, and Fabian P. Alvarez.

The economic burden of influenza among adults aged 18 to 64: A systematic literature review. *Influenza Other Respir Viruses*, 16(3):376–385, MAY 2022.

[3] Catherine A. A. Beauchemin and Andreas Handel. A review of mathematical models of influenza a infections within a host or cell culture: Lessons learned and challenges ahead. *BMC public health*, 11(Suppl 1):S7–S7, 2011.

[4] C Zitzmann and L Kaderali. Mathematical analysis of viral replication dynamics and antiviral treatment strategies: From basic models to age-based multi-scale modeling. *Front. Microbiol.*, 9:1546, 11 July 2018.

[5] Laetitia Canini and Alan S. Perelson. Viral kinetic modeling: State of the art. *J. Theor. Biol.*, 242(2):464–477, 21 September 2006. Draft available on arXiv:q-bio.CB/0505043.

[6] Prasith Baccam, Catherine Beauchemin, Catherine A. Macken, Frederick G. Hayden, and Alan S. Perelson. Kinetics of influenza a virus infection in humans. *J. Virology*, 80(15):7590–7599, AUG 2006.

[7] Amanda P. Smith, David J. Moquin, Veronika Bernhauerova, and Amber M. Smith. Influenza virus infection model with density dependence supports biphasic viral decay. *Front. Microbiol.*, 9, JUL 10 2018.

[8] Alex Farrell, Tin Phan, Christopher B. Brooke, Katia Koelle, and Ruian Ke. Semi-infectious particles contribute substantially to influenza virus within-host dynamics when infection is dominated by spatial structure. *Virus Evolution*, 9(1), APR 13 2023.

[9] Hao Hu, Karima Nigmatulina, and Philip Eckhoff. The scaling of contact rates with population density for the infectious disease models. *Mathematical Biosciences*, 244(2):125–134, AUG 2013.

[10] A. M. Elaiw and S. A. Azoz. Global properties of a class of hiv infection models with beddington-deangelis functional response. *Math Method Appl. Sci.*, 36(4):383–394, MAR 15 2013.

[11] Gang Huang, Wanbiao Ma, and Yasuhiro Takeuchi. Global analysis for delay virus dynamics model with beddington–deangelis functional response. *Appl. Math. Lett.*, 24(7):1199–1203, 2011.

[12] Zhidong Teng Hui Miao and Xamxinur Abdurahman. Stability and hopf bifurcation for a five-dimensional virus infection model with beddington–deangelis incidence and three delays. *J. Biol. Dyn.*, 12(1):146–170, 2018. PMID: 29198164.

[13] Jai Prakash Tripathi, Sarita Bugalia, Vandana Tiwari, and Yun Kang. A predator–prey model with crowley–martin functional response: a nonautonomous study. *Natural Resource Modeling*, 33(4), November.

[14] Nilam Kumar A. Dynamic behavior of an SIR epidemic model along with time delay; crowley-martin type incidence rate and holling type II treatment rate. *Int. J. Nonlin. Sci. Num.*, 2019.

[15] Roberts MG. Diekmann O, Heesterbeek JA. The construction of next-generation matrices for compartmental epidemic models. *J. R. Soc. Interface.*, 7(47), 6 June 2010.

[16] Lubna Pinky and Hana M. Dobrovolny. The impact of cell regeneration on the dynamics of viral coinfection. *Chaos*, 27(6):063109, 2017.

[17] Gilberto González-Parra, Filip De Ridder, Dymphy Huntjens, Dirk Roymans, Gabriela Ispas, and Hana M. Dobrovolny. A comparison of RSV and influenza in vitro kinetic parameters reveals differences in infecting time. *Plos One*, 13(2):e0192645, 8 February 2018.

[18] Noah F. Beggs and Hana M. Dobrovolny. Determining drug efficacy parameters for mathematical models of influenza. *J. Biol. Dynamics*, 9(S1):332–346, 9 June 2015.

[19] Molly E. Gallagher, Christopher B. Brooke, Ruian Ke, and Katia Koelle. Causes and consequences of spatial within-host viral spread. *Viruses*, 10(11), 2018.

[20] Catherine Beauchemin. Probing the effects of the well-mixed assumption on viral infection dynamics. *J. Theor. Biol.*, 242(2):464–477, 21 September 2006. Draft available on arXiv:q-bio.CB/0505043.

[21] A. Boianelli, V. K. Nguyen, Ebensen T., K. Schulze, E. Wilk, N. Sharma, and et al. Modeling influenza virus infection: a roadmap for influenza research. *Viruses*, 7:5274–5304, 12 October 2015.